
Article:
Liu, Z.-H. orcid.org/0000-0002-6597-4741, Long, J.-J., Wei, H.-L. orcid.org/0000-0002-4704-7346 et al. (3 more authors) (2025) A zero-sequence current analysis approach for rotating machinery fault diagnosis of induction motor drivetrain based on sparse learning. IEEE Transactions on Power Electronics. pp. 1-11. ISSN 0885-8993

https://doi.org/10.1109/tpel.2025.3542855

12/02/2025 Final Accepted for publication on IEEE Transactions on Power Electronics
Publication Date: 17/02/2025 DOI: 10.1109/TPEL.2025.3542855

A Zero-Sequence Current Analysis Approach for Rotating Machinery Fault Diagnosis of Induction Motor Drivetrain Based on Sparse Learning

Zhao-Hua Liu, *Senior Member*, *IEEE*, Jun-Jie Long, Hua-Liang Wei, Kan Liu, *Senior Member*, *IEEE*, Ying-Jie Zhang, and Xiao-Hua Li

***Abstract*—Fault diagnosis of rotating machinery driven by induction motors has received increasing attention. Current diagnostic methods, which can be performed on existing inverters or current transformers of three-phase induction machines, have become a more economical and reliable alternative to vibration diagnostic methods. Existing references mainly focus on the stator current analysis of single-phase, but most single-phase current analysis methods utilize only a fraction of the total information accessible in the three-phase system. Field experience shows that zero-sequence current has more distinctive fault characteristics compared to single-phase current, and therefore it is better to use in mechanical fault detection and diagnostic tasks. This paper proposes a novel sparse learning-based method for zero-sequence current analysis for induction rotating motor drive fault diagnosis. Firstly, it elaborates and compares the effectiveness of zero-sequence current in revealing fault characteristics compared with single-phase current by analyzing the fault diagnosis mechanism of zero-sequence current. Additionally, the method proposes a correlation entropy-enhanced sparse learning method for the problem of high-frequency noise and interference in the zero-sequence current signals, so as to enhance the learning of the features of the noise-containing signals. The diagnostic efficacy of the proposed method has been verified through experiments on two real datasets.**

***Index Terms*—induction motor, rotating machinery, zero-sequence current, fault diagnosis，sparse autoencoder**

I. INTRODUCTION[1]

THE rotating machinery, as the heart of industrial drive systems, such as rolling bearings and gears, is of crucial importance for system safety and reliability [1]. Under harsh operating environments with high loads and high torque, rotating machinery is highly susceptible to faults. The occurrence of fault can jeopardize the safety and reliability of the equipment, or even causes huge economic losses and casualties [2]. Therefore, efficient and effective fault diagnosis is essential to improve the safety and reliability of industrial rotating machines [3],[4].

Considerable attention has been paid to fault diagnosis methods for induction motor drive systems, where factors and signals used include vibration [5], acoustic emission [6], temperature [7], rotational speed [1] among others. In the existing study, vibration diagnostic methods are commonly used [8]. However, such a method potentially suffers from a few drawbacks due to the following factors: 1) the installation of sensors may be expensive; 2) the installation location is inconvenient or difficult to access, for example, it may be difficult to install sensors to an equipment that has already been put into production; 3) the collected signals are usually susceptible to vibration of coupled components as well as external interference [9]. On the contrary, motors are widely used in industrial production. The stator currents of motors can be obtained directly from the existing frequency converters or current transformers, making motor current signals (MCS) method a non-intrusive, more economical and reliable alternative for fault diagnosis [10].

For MCS-based methods, it is necessary to distinguish between rotating machinery inside the motor (internal rotating components) and rotating machinery of the external drive train (external rotating components) [11]. Extensive research on methods of fault identification of internal rotating components has been done in recent years [12], [13]. Damage of the internal motor bearings directly affects the air gap of the motor and induces vibrations at characteristic frequencies in the motor current. Whereas the failure characteristics of external bearings must be transmitted through torque variations along the drive train, which can greatly weaken its amplitude after experiencing the damping effect of the couplings and the interference of other dynamical processes, and at the same time, the fault-related current signals are very weak and easy to be drowned out in the noise [14]. Therefore, the use of MCS for external rotating components is challenging.

For the purposes of extracting meaningful signatures from weak fault currents, various approaches have emerged, which can be broadly classified into two categories: 1) model-based analysis approaches, 2) data-driven approaches. Model-based methods establish analytical relationships between the model parameters and the physical parameters of the system with a high degree of interpretability [15]. Amplitude-Frequency

Manuscript received November 06, 2024, revised January 15 ,2025 and accepted February 12, 2025. This work was supported in part by the National Natural Science Foundation of China under Grant 62473147, and Grant 61972443, in part by the Hunan Provincial Key Research and Development Project of China under Grant 2022WK2006, and in part by the International Exchanges 2022 Cost Share Programme Between the Royal Society and the National Natural Science Foundation of China (NSFC) under Grant IEC\NSFC\223266.

[1] Z.-H. Liu, J.-J. Long and X.-H Li are with the School of Information and Electrical Engineering, Hunan University of Science and Technology, Xiangtan 411201, China (e-mail: zhaohua.liu@hnust.edu.cn; long@mail.hnust.edu.cn; xiaohua.li@hnust.edu.cn).

H.-L. Wei is with the Department of Automatic Control and Systems Engineering, School of Electrical and Electronic Engineering, University of Sheffield, Sheffield S1 3JD, U.K. (e-mail: w.hualiang@sheffield.ac.uk).

K. Liu is with the College of Mechanical and Vehicle Engineering, Hunan University, Changsha 410082, China (e-mail: lkan@hnu.edu.cn).

Y.-J Zhang is with the College of Computer Science and Electronic Engineering, Hunan University, Changsha 410082, China (e-mail: zhangyj@hnu.edu.cn).

Demodulation Analysis method [16], Iterative Numerical Integration Solution method [17], and Bispectrum Analysis method have been used to highlight the frequency components associated with faults. However, in practice, such approaches can have the following limitations: 1) it is highly dependent on a priori knowledge to build and maintain the model, and 2) it is difficult to build a completely accurate model due to the complexity and uncertainty of the environment. If the model is inaccurate, then decision-making and planning based on the model may create uncertainty and lead to misdiagnosis.

Data-driven techniques such as machine learning methods directly use historical data, their reliance on a priori knowledge of the system of interest can be reduced and thus are more suitable for modern industrial applications. Singh et al. utilized Continuous Wavelet Transform (CWT) to extract stator current fault features, and achieved outer ring fault detection of bearings mounted on load machine [18]. Lee proposed an external bearing fault diagnosis method that utilizes time domain features (TDFs) to reduce training and inference time, and improves model performance by making use of residuals and densely connected structures [19]. Luo et al. applied Variational Mode Decomposition (VMD) to decompose the motor current signal, the energy entropy of the resulting intrinsic mode functions (IMFs) and five time-frequency features were selected as inputs to the Probabilistic Neural Network (PNN) classifier for fault diagnosis of wind turbine gearboxes [20]. The aforementioned methods have yielded remarkable results, but there are limitations in terms of stability and generalizability. Specifically, all these methods are designed based on multiple signal preprocessing methods in the time-frequency domain, requiring a large amount of a priori knowledge or diagnostic expertise. The performance of feature engineering and machine learning models greatly affects the accuracy and generalization ability of diagnostics. Deep learning (DL) methods, due to their powerful ability to automatically learn useful information and feature representations, become an effective means to for signal processing and feature extraction [21]. More attention is being paid to automatic feature learning, including Convolutional Neural Network (CNN) and Autoencoder (AE), which have been used for machine state identification and effective current signal processing [9].

In [11], two-phase current signals were transformed into 2D image signals and fed into a CNN model, then fused the learned two-phase information for fault classification. Wang et al. designed a CNN-based feature fusion model, which fully fused the complementary characteristics extracted from current and vibration signals to realize the fault diagnosis of bearings [22]. Hou et al. designed a CNN-based current fault diagnosis model that used a comb filter as a convolutional layer to realize the diagnosis task under limited sample conditions [23]. Cipollini et al. utilized two-phase current signals as inputs to the stack AE to achieve diagnosis of two bearing faults [24]. Sun et al. introduced a noise cancellation method to obtain the residual current, the features were then extracted from the residual current data using the stack AE and finally fault diagnosis of the motor was realized [12].

Literature reviews show that deep learning methods outperform other state-of-the-art fault detection methods in some applications, but there are still some challenges that limit their application. For example, the performance of the above methods often depends on the design of the network architecture and the quality of the fault data used. These methods may not be easily implemented and used for complex industrial applications [25]. If the network is not well designed or the training data are not good enough, the resulting models may not work well. Therefore, it is particularly important to develop effective feature learning and enhancement methods to improve fault feature extraction for noisy current signals.

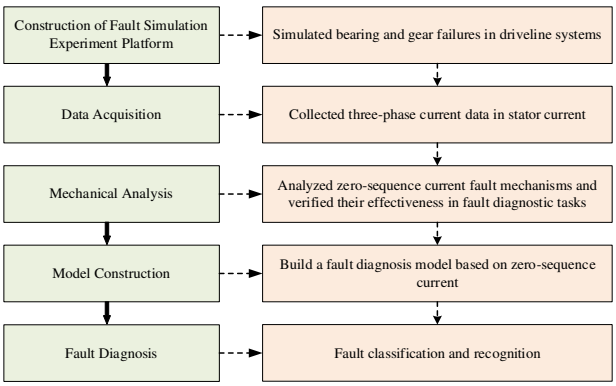

Fig. 1. The block diagram of the proposed fault diagnosis approach.

It is worth noting that all papers reviewed above focus on analyzing single-phase current signals. In fact, most existing current diagnostic methods are also based on single-phase current signals. However, the information carried by each stator current in a three-phase system can vary slightly from phase to phase due to the presence of initial phase shifts, amplitude and/or phase imbalances, high-frequency noise components, and measurement errors. Therefore, methods that rely solely on single-phase current analysis can only utilize a small fraction of the total available information in a three-phase system and cannot fully exploit the potential value of the data [26].

Given the wide range of applications of three-phase rotating motors in complex industrial equipment such as wind turbines, automobile manufacturing and metallurgical machinery, it is particularly important to comprehensively consider the three-phase current parameters in the condition monitoring of three-phase systems. In particular, the zero-sequence current (ZSC), as a superposition of the three-phase currents, contains a wealth of information about the symmetry of the machine. A deviation from the normal state may indicate a potential fault condition, making the zero-sequence current component an extremely sensitive indicator for monitoring machine operating conditions.

Bearing the above consideration in view, this work tasked to improve the performance of extracting weak fault features from motor current signals. In doing so, a correlation entropy-enhanced sparse learning method (CESL) is proposed to handle zero-sequence current signals. Through this perspective, it targeted to dig deeper into the fault characteristics in the current signals and provide a more accurate and comprehensive basis for the fault diagnosis of rotating machinery. The block diagram of the proposed fault diagnosis approach is shown in Fig. 1.

The main contributions of the paper are outlined below:

1) A new fault diagnostic scheme using zero-sequence

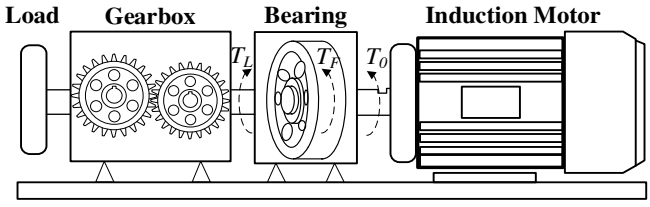

Fig. 2. The schematic diagram of the induction motor drive system.

current is introduced and its effectiveness in revealing fault characteristics is analyzed.

2) An intelligent fault diagnosis approach based on three-phase current signals is proposed, which can automatically and efficiently extract representative features from weak current data, and eliminate the need for traditional signal processing methods and expert experience.

3) Considering the existence of high-frequency and periodic noise in the motor stator current, a correlation entropy-enhanced sparse autoencoder loss function is designed to strengthen the ability of feature representation and learning.

The rest of the paper is organized as follows. In Section II, the fault mechanism of current signals is analyzed, Section III describes the details of the suggested model, and the validity of the method is verified by experiments on two datasets in Section IV. The paper is summarized in Section V.

II. Analysis of Motor Current Mechanism

A. Analysis of stator currents

In rotating machinery, when a malfunction (e.g., bearing failure, gear breakage) occurs, additional torque fluctuations may be generated [27]. These events cause fluctuations in the air-gap magnetic chain, which result in the stator current signals being modulated in both amplitude and phase, thereby emerging new frequency components [23]. To facilitate the analysis process, the following provides an example of a bearing failure.

For the bearing current detection model, it can be roughly divided into two components: the rotor radial model and the torque transmission model. The radial model was initially proposed by Schoen, where it was assumed that the motor stator generates a rotational eccentricity when the bearing is in a faulty state, and this eccentricity leads to the stator induced current cyclic change [28]. However, this model does not take into account the torque variation, so it is only suitable for fault diagnosis of internal rotating components. Another model is the torque transmission model, its mechanism is as follows: when the bearing fails, the ball passing through the defective parts of the inner and outer rings of the bearing generates transient fluctuations of torque, causing changes in the stator current signal [29].

It was shown that torque fluctuations arising from bearing faults are the main cause of the changes in the stator current through mechanical analysis [30]. The torque transmission model can explain not only the motor itself, but also the fault induction principle of the drive train bearing. Thus, this paper mainly focuses the stator current induction principle of bearing failure with the torque transmission model. To illustrate the effect of bearing failure on the current signal, a schematic diagram of an electromechanical drive train is depicted in Fig. 2.

When the bearing breaks down, the load torque consists mainly of a constant component T_0 and an oscillating component at the characteristic frequency f_c [29]. The higher order terms are neglected and only the fundamental terms are considered as follows:

$$T_{\text{Load}}(t) = T_0 + T_c \cos(2\pi f_c) \tag{1}$$

where T_c is the amplitude of the oscillations associated with the severity of the fault.

The change in rotor speed and rotor angular position due to torque oscillations at the characteristic frequency lead in turn to phase modulation of the rotor magnetomotive force (MMF) in the stator reference frame. As a result, the flux density in the motor air gap will change and the additional flux causes the stator current to generate an extra frequency. The stator current can be expressed as:

$$\begin{aligned} I(t) &= i_{st}(t) + i_{rt}(t) \\ &= I_{st}\ sin(\omega_s t + \phi_s) + I_{rt}\ sin\left(\omega_s t + \beta\ cos(\omega_c t)\right) \end{aligned} \tag{2}$$

where terms $i_{st}(t)$ and $i_{rt}(t)$ are the stator current components generated by the stator magnetomotive force and rotor magnetomotive force respectively; ω_s is the angular velocity associated with the power supply, and β is the modulation index, a healthy case is obtained for β=0.

The main principle of stator current detection for bearing faults can be found in [29]. The effect of torque variations causing changes in the motor current is a phase modulation of the current spectrum:

$$f_{BF} = \left| f_s \pm k f_c \right| \tag{3}$$

where k is the harmonic order, k=1,2,3…, f_c is the characteristic frequency of bearing faults.

B. Analysis of zero-sequence current

Theoretically, in a healthy operating condition, the phase current is defined as:

$$i_H(t) = I_n cos(2\pi n f_s)t = I_n cos(n\omega_s)t \tag{4}$$

where f_s is the power supply frequency. And in a three-phase system, the currents have symmetry, i.e., the three-phase currents are equal in amplitude and 120° out of phase:

$$i_{zsc}(t) = i_{ph\_a}(t) + i_{ph\_b}(t) + i_{ph\_c}(t) \tag{5}$$

The ZSC arises from the instantaneous sum of the three-phase currents and hence the ZSC is zero. Considering the effect of bearing failure on stator current, (4) is modified as follows:

$$i_F(t) = \sum_{n=1}^{\infty}\left[I_n \cos(n\omega_s)t + \sum_{k=1}^{\infty} I_k \cos(n\omega_s \pm k\omega_f)t \right] + N(t) \tag{6}$$

where $N(t)$ represents the Gaussian noise arising from sensor measurement.

Therefore, for each phase current

$$\begin{aligned} i_{aF}(t) &= \sum_{n=1}^{\infty}\left\{ I_{1n}\cos(n\omega_s t) + \sum_{k=1}^{\infty} I_{1k}\cos(n\omega_s \pm k\omega_c)t \right\}) + N_1(t) \\ i_{bF}(t) &= \sum_{n=1}^{\infty}\left\{ I_{2n}\cos\left[n(\omega_s t - \frac{2\pi}{3}) \right] + \sum_{k=1}^{\infty} I_{2k}\cos\left[n(\omega_s t - \frac{2\pi}{3}) \pm k\omega_c t \right] \right\} + N_2(t) \\ i_{cF}(t) &= \sum_{n=1}^{\infty}\left\{ I_{3n}\cos\left[n(\omega_s t - \frac{4\pi}{3}) \right] + \sum_{k=1}^{\infty} I_{3k}\cos\left[n(\omega_s t - \frac{4\pi}{3}) \pm k\omega_c t \right] \right\} + N_3(t) \end{aligned} \tag{7}$$

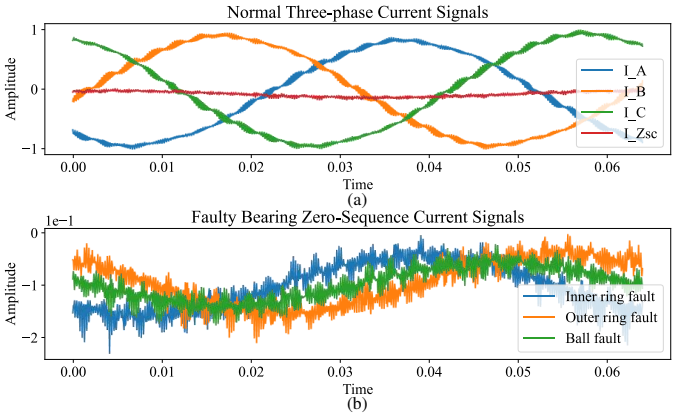

Fig. 3. True motor current under normal and fault conditions. (a) Normal three-phase current signals. (b) Faulty bearing zero-sequence current signals.

Firstly, when rotating machinery fails, such as damage to bearing rolling elements or missing and broken teeth in gear components, it leads to uneven load distribution, so that the three phases are not completely symmetrical, as a result of which (5) is not at zero. Secondly, the failure of rotating machinery can cause mechanical vibration and impact, which in turn is transmitted to the stator of the motor. In the current signal, the mechanical vibration and impact will be manifested as an increase in the ZSC, and different faults may also lead to differences in the phase of the ZSC. This is depicted in Fig. 3. Observing Fig. 3(a), it can be seen that when the machinery is operating in a normal state, the zero-sequence current is almost zero and is at a very low level. However, as shown in Fig. 3(b), once a fault occurs in the machinery, the zero-sequence current will show a clear trend of increase, accompanied by the generation of phase difference.

Therefore, by monitoring the magnitude of the ZSC, it is possible to determine whether a fault exists in the rotating machinery.

C. Spectral analysis

The spectrograms of single-phase current signal and ZSC signal is plotted to further elaborate the above fault mechanism, as shown in Fig. 4. Taking the induction motors speed (S=1000 rpm) as an example, the current mechanism of inner ring failure and outer ring failure of the bearing is analyzed. The bearing parameters are shown in Table I.

The rotational frequency can be calculated as:

$$F_r = \frac{S}{T} = \frac{1000}{60} = 16.7\ Hz \tag{8}$$

where T is the number of seconds contained in each minute.

The failure frequency of the inner ring can be calculated as:

$$F_i = \frac{nF_r}{2}\left(1+\frac{d}{D}\cos\phi\right) = \frac{9*16.7}{2}*\left(1+\frac{25}{52}*\cos\left(0^\circ\right)\right) = 111.28\ Hz \tag{9}$$

The failure frequency of the out ring can be calculated as:

$$F_o = \frac{nF_r}{2}\left(1-\frac{d}{D}\cos\phi\right) = \frac{9*16.7}{2}*\left(1-\frac{25}{52}*\cos\left(0^\circ\right)\right) = 39.02\ Hz \tag{10}$$

The current spectra for the outer ring fault (OF) are shown in Fig. 4(a) and Fig. 4(c). For single-phase currents, the amplitude of the fault frequency is weak and shows essentially no peaks. Zooming in on the spectrogram reveals tiny spikes

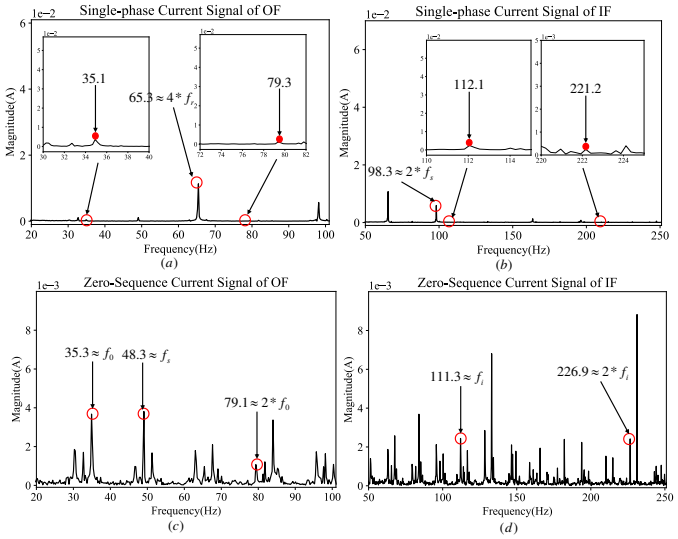

Fig. 4. Illustrations of the spectra of inner and outer ring faults. (a) Single-phase current of outer ring fault. (b) Single-phase current of inner ring fault. (c) zero-sequence current of outer ring fault. (d) zero-sequence current of inner ring fault.

TABLE I
BEARING-RELATED PARAMETERS

Parameter	Value	Parameter	Value
Number of balls(n)	9	Pitch diameter(D)	52mm
Ball diameter(d)	25mm	Contact angle(β)	0

at 35.1 Hz and 79.3 Hz. Whereas in the spectrogram of ZSC, it can be found that there are obvious peaks at 35.3 Hz and 79.1 Hz. The spectra of the current for the inner ring fault (IF) are shown in Fig. 4(b) and Fig. 4(d). For single-phase current, two small peaks are found at 112.1 Hz and 221.2 Hz. For ZSC, fault frequencies of 111.3 Hz and 226.9 Hz are clearly observed.

In summary, compared to single-phase current, ZSC has more distinctive fault characteristics and is better to use for mechanical fault detection and diagnosis. In addition, the diagnosis using the spectrum signal may be inaccurate due to the fact that the noise signal still exists in the ZSC signal and the fault signature frequency in practical applications can differ from the theoretical value.

Therefore, using feature extraction techniques is necessary and more effective in enhancing the fault features for better diagnosis.

III. THE PROPOSED CESL NETWORK

A. The proposed CESL network

The traditional sparse autoencoder (SAE) learns features from the original data by encoding and decoding. Encoding is a process of encoding the input data into features, whereas decoding is a process of decoding the features into outputs for input reconstruction [31].

Let $X = [x_1, x_2, ..., x_n]^T \in R^{n\times m}$ be unlabeled data used in the encoding process, and z_i be data used in the hidden layer which can be obtained by the encoding function $f_e()$ used in the decoding process. The decoder uses a mapping function

$g_d()$ to reconstruct the data $\hat{X}$,which is formulated in (11):

$$\begin{cases} Z_i = f_e(X) = \sigma_f(WX + b) \\ \hat{X} = g_d(Z) = \sigma_g(W'Z + b') \end{cases} \tag{11}$$

where σ_f and σ_g are two nonlinear activation functions, W and W' are the weight matrix, b and b' are the bias vector.

SAE seeks to optimize parameters $\omega=\{W, b, W', b'\}$ by minimizing the error between $\hat{X}$ and X, and the process of training is to minimize the cost function:

$$\begin{aligned} J(\omega) &= J_{MSE}(\omega) + \beta J_{KL}(r\|\hat{r}) \\ &= \frac{1}{n}\sum_{i=1}^{n}\left(\frac{1}{2}\left\|\hat{X}_i - X_i\right\|^2\right) + \beta\sum_{i=1}^{n_l}\left(r\log\frac{r}{\hat{r}_i} + (1-r)\log\frac{1-r}{1-\hat{r}_i}\right) \end{aligned} \tag{12}$$

where $J_{MSE}(\omega)$ is the reconstruction error; $J_{KL}(r||\hat{r})$ is the sparse penalty term defined by the KL divergence (distance), β is the sparse weight, n_l is the number of hidden layers, and r is a sparse parameter. The purpose of $J_{KL}(r||\hat{r})$ is to keep the average activity of hidden neurons small to ensure that more features can be learned.

Based on SAE, we propose to use CESL for extracting more representative features from fault signals. The diagram of the CESL model is shown in the Fig.5. The differences between CESL and traditional SAE are as follows.

In SAE, the mean square error (MSE) is traditionally considered as the loss function. However, MSE lacks robustness for feature learning. To improve the ability of SAE, an integrated loss function, comprising three components, namely, correlation entropy term $J_{MSE}(\omega)$, divergence (distance) term $J_{KL}(r||\hat{r})$ and a weighting term $J_{weight}(\omega)$, is used in this paper which is defined as follows:

$$J_{new}(\omega) = -J_{MC}(\omega) + \beta J_{KL}(r\|\hat{r}) + \lambda J_{weight}(\omega) \tag{13}$$

where the explanations of three terms are given below.

Firstly, the correlation entropy function is introduced to address the limitations of the traditional reconstruction loss function. The correlation entropy is a generalized similarity metric of two random variables A and B, it can be used as an indicator of the error between $\hat{X}$ and X [32]. It is defined as:

$$V_\sigma(A,B) = E\left[\kappa_\sigma(A-B)\right] \tag{14}$$

where $\kappa_\sigma(\cdot)$ is a kernel function that satisfies Mercer's theory, and $E(\cdot)$ is the expectation.

Unlike MSE, correlation entropy is more robust to outliers and noise. Since correlation entropy uses a kernel function to measure the similarity between predicted and target values, it is less sensitive to outliers. This makes correlation entropy better for handling data with noise or outliers. The estimated correlation entropy is calculated by (14):

$$\hat{V}_\sigma(A,B) = \frac{1}{n}\sum_{i=1}^{n}\kappa_\sigma(a_i - b_i) \tag{15}$$

In this work, the Gaussian kernel function is used, which is defined as:

$$\kappa_\sigma(\cdot) = \frac{1}{\sqrt{2\pi}\sigma}\exp\left(-\frac{(a_i-b_i)^2}{2\sigma^2}\right) \tag{16}$$

where σ is the kernel size. Then, the correlation entropy loss

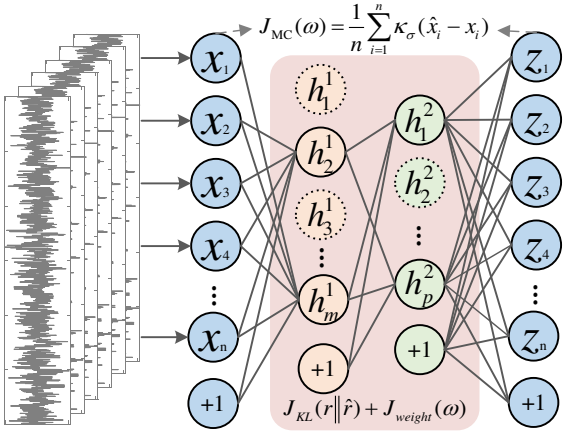

Fig. 5. The proposed CESL network.

function is designed to replace the traditional MSE, and the formula is shown below:

$$J_{MC}(\omega) = \frac{1}{n}\sum_{i=1}^{n}\kappa_\sigma(\hat{x}_i - x_i) \tag{17}$$

To further enhance the feature learning ability of the designed network model, a non-negative constraint term is introduced into the cost function, which makes the model parameters sparser and thus enables the learning of more representative features from high-dimensional data [33], denoted as

$$J_{weight}(\omega) = \frac{\lambda}{2}\sum_{l=1}^{k-1}\sum_{j=1}^{n_l}\sum_{i=1}^{n_{l-1}}G(W_{ij}^l) \tag{18}$$

with

$$G(W_{ij}^l) = \begin{cases} (W_{ij}^l)^2, & W_{ij}^l > 0 \\ 0, & W_{ij}^l \le 0 \end{cases} \tag{19}$$

where λ is weighting coefficients, k is the number of network layers. n_l is the number of nodes in layer l.

D. The procedure of the CESL method

The diagram of implementation procedure of the proposed CESL diagnostic approach is shown in Fig. 6, which include the following steps.

1) *Data acquisition*: To design rotating machines fault experiments, based on which to collect three-phase current data, and get zero-sequence current signals.

2) *Data preprocessing*: To remove random noise and high frequency components from the signals; to preprocess the raw data using a mean filtering technique. To segment the processed data using a time shift window scheme. Finally, to normalize the preprocessed data.

3) *The CESL structure establishment*: To initialize the network parameters, fine-tune the network parameters according to the proposed integrated error function model, and complete the entire training process with the goal of minimizing $J_{new}(\omega)$.

4) *Fault classification:* To perform fault diagnosis by putting test samples into the trained CESL network models to learn representative features, which are then fed into the *SoftMax* classifier.

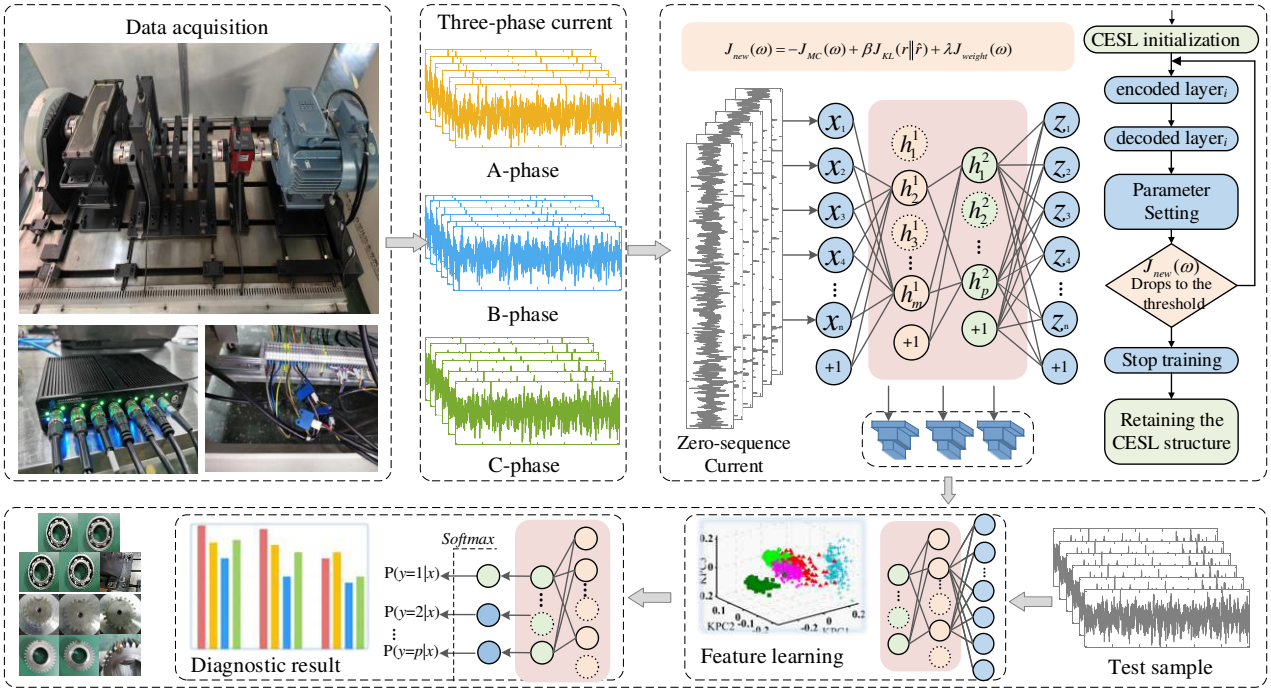

Fig. 6. The framework of the proposed CESL.

IV. Case Verification

A. Experimental Settings

To evaluate the performance of the suggested approach, a mechanical fault simulation test rig was constructed as shown in Fig. 7. It comprises a three-phase asynchronous motor and a mechanical transmission device, in which the mechanical transmission device includes a variety of engineering machinery used in the main transmission parts, including bearings, gears, couplings, drive shafts and so on. Some details of the parameters of the asynchronous motor are shown in Table II.

In our experiments, a frequency converter (Model: FD9A0-MS43ANSAA) is used for precise speed control of the motor, and a current sensor (Model: CSM020GB) is used to monitor the motor current in real time. Simulations for different loads were carried out by applying different radial load forces. In addition, we installed acceleration sensors (Model: HD-YD-232) on the monitored components to capture vibration signals. Eventually, these data were collected synchronously by a multi-channel data acquisition device to ensure the integrity and accuracy of the data. The sampling frequency of the data acquisition card is 16K, enabling sufficient frequency resolution to capture the characteristic frequency of fault generation. Taking into account data adequacy and processing efficiency, we selected a sampling time of 4 seconds. The working condition of the motor is 2,000 rpm and the radial loading force is 1400 N to simulate the bearing load under normal operating conditions. A total of three sets of data were collected.

Parameter settings: The CESL model was constructed to determine the network structure by analyzing the trend of the novel integrated error function $J_{new}(\omega)$. The training period for the experiment is 50, and the batch size is 128.

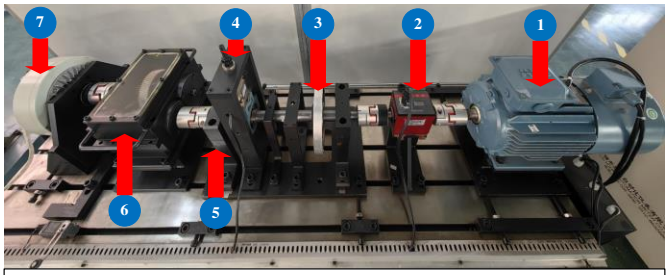

1: Driving motor 2: Torque and speed sensor 3: Balance wheel
4: Radial loading device 5: Rolling bearing seat
6: Fault simulation gearbox 7: Loading system

Fig. 7. Mechanical fault simulation test rig.

TABLE II
Induction Motor Parameters

Parameter	Value	Parameter	Value
Rated power	3 kW	Stator Connection	Y
Rated current	6.58 A	Rated frequency	50 Hz
Rated voltage	380 V	Pole-pair number	1

TABLE III
Model Parameter

Description	Symbol	Value
The structure of the CESL	-	1024-256-100-6
Gaussian kernel size	σ	1
Sparsity penalty weight	β	0.03
Sparsity parameter	r	0.01
Non-negative constraint weight	λ	0.1
Learning rate	-	0.001

The window length is fixed at 1024 and the moving step is 100. the number of samples in each category is 1881. The optimizer of the network is Adam. The main parameters of the model are shown in Table III.

Comparison methods: To test and verify the model performance, we considered the following eight methods for comparison purposes.

a) **SP-CESL**: As with conventional current diagnostics, single-phase currents are directly used as inputs to the CESL.

b) **SC-CESL**: The three-phase currents are first time-shifted and synchronized, then integrated and squared to obtain the current residual signal. Finally, the current residual signal is fed into the CESL. Residual currents are obtained in [13].

c) **ZS-SAE**: It adopts ZSC data as input to a standard SAE. The parameters are consistent with the proposed method.

d) **ZS-SVM**: It adopts the ZSC data and then use SVM for fault classification. Build and apply SVM models by calling the Scikit-learn library. A Gaussian kernel, with penalty coefficient C=1, is used in the SVM model.

e) **ZS-MSCNN**: It takes the ZSC data and then uses a multiscale CNN for subsequent feature extraction and classification. The configuration of the CNN is as follows. The convolutional kernels are 7, 5, and 3, respectively, and the corresponding number of output channels are all set to 32, the pooling kernel size is 2, the step size is 2. The nonlinear transformation is performed using the *ReLU* activation function, and the classification results are obtained through the fully connected layer. The learning rate is 0.001.

f) **ZS-GRU**: It adopts ZSC data as input to Gated Recurrent Unit (GRU). The hidden layer dimension of GRU is 128 and the number of layers is 4. The learning rate is 0.001.

g) **VS-CESL**: It adopts vibration signal data as input to CESL.

All the experiments were repeated five times and their mean value was taken as the final experimental result to reduce the effect of chance.

B. Bearing Fault Experiment

The experiment is as follows: four bearings with different failure types were used for the experiment. The specific setup and procedure of the experiment ensured that all bearings were tested under the same conditions. In addition, a set of experiments were added for bearing seat misalignment. Fig. 8. clearly shows the failure areas of the bearings. Table IV provides a detailed description of the five bearing failure types.

Diagnostic result analysis: The diagnostic results for the six bearing conditions are shown in Table V, where it can be observed that the proposed method significantly outperforms other methods in terms of accuracy (**98.48%**), standard deviation (0.23%), and run time (12.49 s), and can meet the field requirements of industrial applications, which can meet the field requirements for industrial applications. Overall, our approach achieves great the best diagnostic performance for the six bearing faults, specifically:

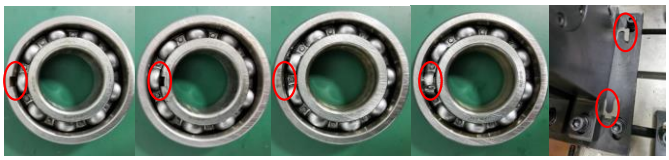

(a) (b) (c) (d) (e)

Fig. 8. Rolling bearings with different faults.

TABLE IV
ROLLING BEARINGS WITH DIFFERENT FAULTS

Index	Class	Label
	Normal	NR
(a)	Outer ring crack failure	OF
(b)	Inner ring crack failure	IF
(c)	Ball pitting failure	BF
(d)	Cage broken failure	CF
(e)	Misalignment failure	MF

1) Advantages of ZSC

For the current-based approach, if only the single-phase current is used, the accuracy of the SP-CESL approach is 16.57%. However, if the ZSC is taken as an input to the network, the accuracy increases significantly. This can be explained by the fact that single-phase current does not characterize mechanical faults significantly, whereas the ZSC carries all the information of the three-phase current, which is more suitable for monitoring the condition of machinery.

If the integration of stator synchronized current method is used, the fault information is still not sensitive enough to achieve a better diagnostic performance, even if the SC-CESL model eliminates the noise to a certain extent.

Compared with the vibration-based method, the accuracy (99.54%) of VS-CESL is slightly higher than that of our proposed method, but the method has limitations in practical applications. From the perspective of applicability, the proposed method is superior to VS-CESL.

2) Advantages of the proposed CESL

Compared with the standard SAE, our approach has improved feature extraction capability. The superiority of the new approach is attributed to the better adaptability of the designed integrated loss function, which is more robust in dealing with outliers and background noise of the motor current signals. Moreover, the introduced non-negative constraint term can further enhance the sparsity, making the

TABLE V
A COMPARISON OF DIFFERENT METHODS

Method	Accuracy (%)	Standard deviation	Precision	Recall	F1_score	Time (s)
SP-CESL	16.57%	1.31%	0.1825	0.1670	0.1086	9.77
SC-CESL	43.12%	0.43%	0.5030	0.4309	0.4033	11.92
VS-CESL	99.54%	0.31%	0.9957	0.9955	0.9955	13.15
ZS-SAE	86.50%	2.3%	0.8675	0.8667	0.8648	8.84
ZS-SVM	93.2%	0.71%	0.9330	0.9317	0.9320	2.25
ZS-GRU	96.09%	0.95%	0.9627	0.9617	0.9616	10.23
ZS-MSCNN	98.74%	0.47%	0.9877	0.9875	0.9875	17.23
Proposed	**98.48%**	**0.23%**	**0.9851**	**0.9851**	**0.9851**	**12.49**

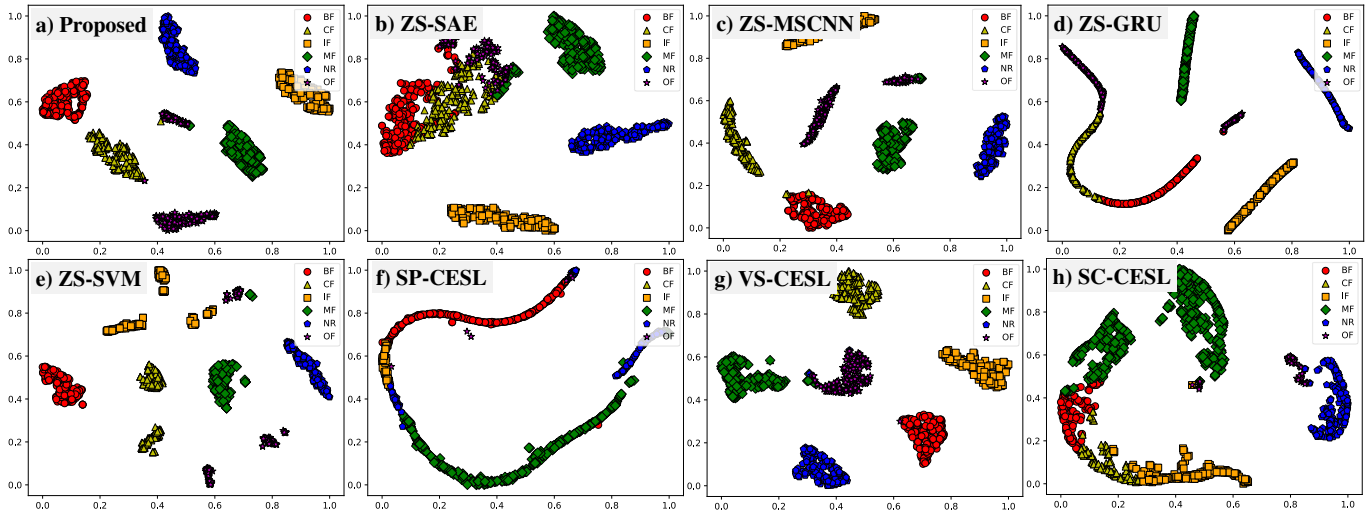

Fig. 9. t-SNE visualization results.

model more focused on learning positive feature representations.

Compared to GRU and MSCNN methods, our method balances robustness and computational efficiency. This is due to the fact that our method is able to capture the essential features from the noise contaminated signals through the correlation entropy-enhanced sparse learning approach. In contrast, although the MSCNN method achieves good performance by using convolutional kernels of different scales for multi-scale feature extraction of current signals, its performance highly depends on the design of the network architecture and the number of samples, and the associated model training is usually time consuming.

The GRU method, on the other hand, mainly controls the flow of information through a gating mechanism, but it does not impose an explicit constraint on the sparsity of features, therefore its feature extraction capability is relatively weak.
The performance of traditional machine learning methods (SVM) is highly dependent on the quality of pre-determined features and may be difficult to generalize across different fault diagnosis tasks. In contrast, our method can adaptively learn representative features from the input data and show better diagnostic performance.

To demonstrate the signature extraction capability of the proposed approach, the t-SNE technique is utilized to visualize the fault classification results [34]. The principle of this algorithm is to downscale the high-dimensional data to a low-dimensional space through nonlinear mapping to achieve better visualization, and meanwhile maintains the local structure of the data. Fig. 9. shows the visualization results of the eight methods, from which we can see that the proposed method can distinguish the six bearing states clearly. These show that the features extracted by the suggested approach are highly beneficial for the bearing condition monitoring task.

C. Gearing Fault Experiment

In this section, failure simulation has been carried out on planetary gearboxes with three failure faults, each on the sun wheel and planetary wheel as shown in Fig. 10. Table VI details the seven types of gear failures.

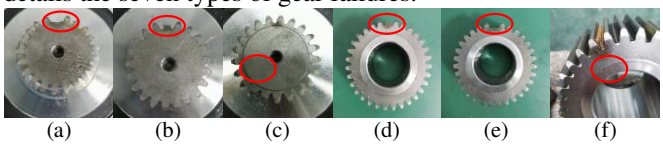

Fig. 10. Gearings with different faults.

TABLE VI
ROLLING BEARINGS WITH DIFFERENT FAULTS

Index	Class	Label
	Normal	NR
(a)	Sun Gear Broken Teeth	SGBT
(b)	Sun Gear Missing Teeth	SGMT
(c)	Sun Gear Crack	SGC
(d)	Planetary Gear Broken Teeth	PGBT
(e)	Planetary Gear Missing Teeth	PGMT
(f)	Planetary Gear Crack	PGC

TABLE VII
A COMPARISON OF DIFFERENT METHODS

Method	Accuracy (%)	Standard deviation	Precision	Recall	F1_score	Time (s)
SP-CESL	40.03%	3.23%	0.3509	0.4022	0.3374	10.77
SC-CESL	60.03%	1.04%	0.5313	0.5984	0.5347	8.89
VS-CESL	98.46%	0.48%	0.9847	0.9851	0.9848	15.36
ZS-SAE	97.55%	0.82%	0.9755	0.9752	0.9752	10.24
ZS-SVM	98.35%	0.18%	0.9829	0.9831	0.9829	2.38
ZS-GRU	94.51%	0.85%	0.9488	0.9449	0.9412	12.25
ZS-MSCNN	99.96%	0.06%	0.9996	0.9996	0.9996	20.05
Proposed	**0.9998**	**0.03%**	**0.9998**	**0.9998**	**0.9998**	**14.7**

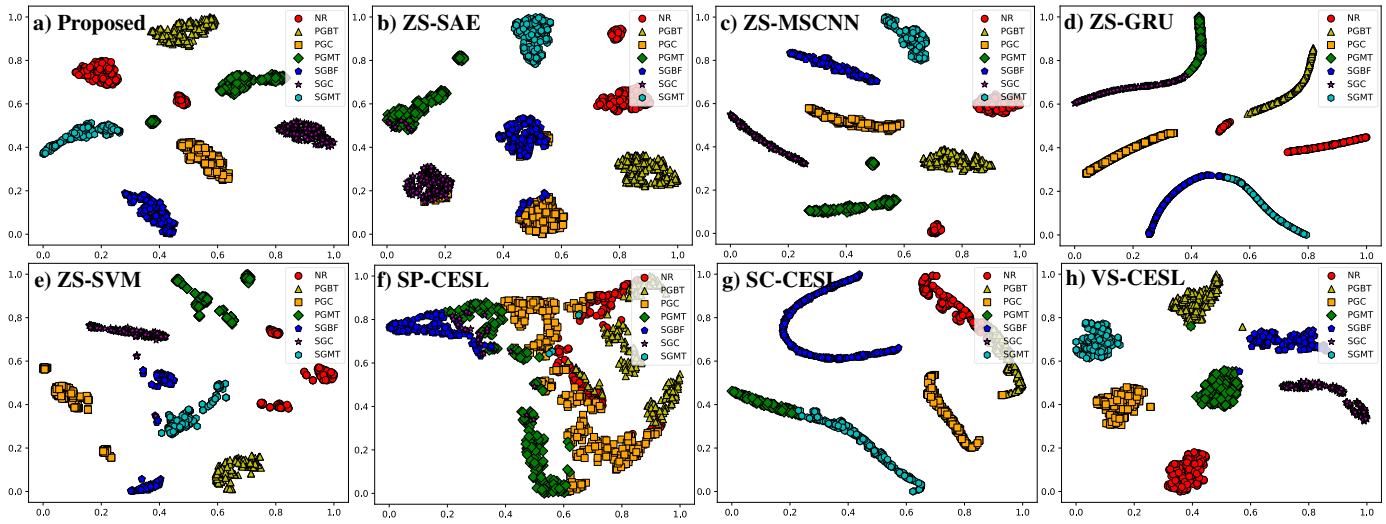

Fig. 11 t-SNE visualization results.

Diagnostic result analysis: Table VII illustrates the accuracy of eight different methods. It can be seen from the table that the proposed method has the best performance with an average accuracy of **99.98%**.

In terms of the feature extraction method, the accuracy (99.96%) of the MSCNN method is close to that of the proposed model, but its training time is much higher. The reason for the much higher accuracy of the SVM method (compared to the previous experiment) may be explained that gear faults are more sensitive to the features extracted manually.

The t-SNE method is used for analyzing the experimental results. As can be seen from the Fig. 11, our method has clear boundaries between classes and the classification is very satisfactory. Combining the two experiments of bearing and gear, our proposed method takes into account the training efficiency and real-time demand while maintaining high accuracy, providing an efficient and reliable solution in the field of rotating machinery fault diagnosis, which is promising and desirable for practical applications.

D. Hyperparameter analysis

We analyzed the effect of the Gaussian kernel parameter and the sparsity parameter on the classification accuracy of the model, tested on both bearing and gearbox datasets.

Gaussian kernel parameter: controls the sensitivity of the loss function to distance and affects the robustness of the model. We tested different values of the Gaussian kernel parameters (0.1,0.5,1,1.5,1.5,2). The optimal parameters are in the range between 0.5 to 1.5. As shown by the solid lines in Fig. 12.

Sparse penalty coefficients are crucial for the quality of extracted features and affect the generalization of the model. We tested several different sparse penalty values (0.01,0.03,0.05,0.07,0.09,0.1). It turned out that the optimal parameters are between 0.01 and 0.05. In summary, the proposed method is not highly sensitive to parameter variations; it shows robust classification performance.

The diagnostic experiments were performed on an NVIDIA GeForce RTX 4070 GPU and the programming language is Python.

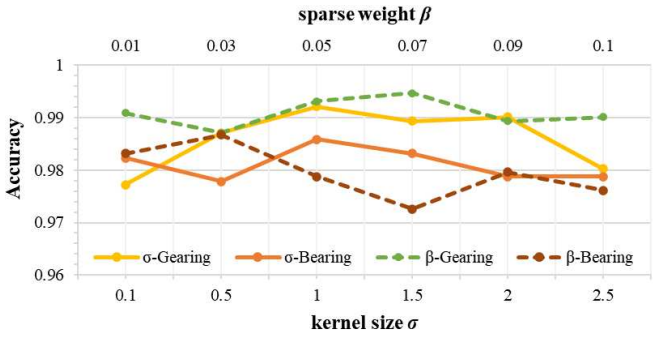

Fig.12. Effect of different parameters on accuracy.

V. Conclusion

The existing current-based methods cannot provide good performance and suffer from weak signal amplitude and low signal-to-noise ratio. To overcome these drawbacks, this paper investigates the problem of fault diagnosis of rotating machinery based on ZSC signals, by analyzing the fault mechanism of current. The ZSC contains rich fault information compared to that of single-phase current and is better to use for monitoring the safety of mechanical systems.

A correlation entropy-enhanced sparse feature learning method is designed, which can automatically and efficiently extract fault characteristics without the need of manual interference. One of the advantages of the new method is that it has good robustness to with noisy signals. The method is applied to fault diagnosis of bearings and gearboxes in transmission systems. The experimental results show that the proposed rotating machinery fault diagnosis method has good application prospects.

In the future, we plan to extend the pioneering approach to a wider range of electromechanical systems. In addition, due to the scarcity and variety of fault data, and the differences between testbed data and actual data, there is a need to take these differences into account and utilize transfer learning to improve the model capability.

REFERENCES

[1] X. Chen, and Z. Feng, "Tacholess speed estimation for rotating machinery fault diagnosis of induction motor drivetrain," *IEEE Transactions on Power Electronics*, vol. 39, no. 4, pp. 4704-4713, April 2024.

[2] S. Yu, S. Pang, J. Ning, M. Wang, and L. Song, "ANC-Net: A novel multi-scale active noise cancellation network for rotating machinery fault diagnosis based on discrete wavelet transform," *Expert Systems with Applications,* vol. 265, pp. 125937, 2025.

[3] Z. Wang, M. Zhang, H. Chen, J. Li, G. Li, J. Zhao, L. Yao, J. Zhang, and F. Chu, "A generalized fault diagnosis framework for rotating machinery based on phase entropy," *Reliability Engineering & System Safety,* vol. 256, pp. 110745, 2025.

[4] Y. Abudurexiti, G. Han, L. Liu, F. Zhang, Z. Wang, and J. Peng, "Graph-guided higher-order attention network for industrial rotating machinery intelligent fault diagnosis," *IEEE Transactions on Industrial Informatics,* vol. 20, no. 2, pp. 1113-1123, 2023.

[5] Z. Zhu, Y. Lei, G. Qi, Y. Chai, N. Mazur, Y. An, and X. Huang, "A review of the application of deep learning in intelligent fault diagnosis of rotating machinery," *Measurement,* vol. 206, pp. 112346, 2023.

[6] A. Glowacz, "Acoustic based fault diagnosis of three-phase induction motor," *Applied Acoustics,* vol. 137, pp. 82-89, 2018.

[7] P. Ong, A. J. Koshy, K. H. Lai, C. K. Sia, and M. Ismon, "A deep learning approach for health monitoring in rotating machineries using vibrations and thermal features," *Decision Analytics Journal,* vol. 10, pp. 100399, 2024.

[8] B. A. Tama, M. Vania, S. Lee, and S. Lim, "Recent advances in the application of deep learning for fault diagnosis of rotating machinery using vibration signals," *Artif. Intell. Rev.,* vol. 56, no. 5, pp. 4667-4709, 2023.

[9] G. Niu, X. Dong, and Y. Chen, "Motor fault diagnostics based on current signatures: a review," *IEEE Transactions on Instrumentation and Measurement*, vol. 72, pp. 1-19, 2023.

[10] D. Lu, W. Qiao, and X. Gong, "Current-based gear fault detection for wind turbine gearboxes," *IEEE Transactions on Sustainable Energy,* vol. 8, no. 4, pp. 1453-1462, 2017.

[11] D. T. Hoang, and H. J. Kang, "A motor current signal-based bearing fault diagnosis using deep learning and information fusion," *IEEE Transactions on Instrumentation and Measurement,* vol. 69, no. 6, pp. 3325-3333, 2019.

[12] M. Sun, H. Wang, P. Liu, Z. Long, J. Yang, and S. Huang, "A novel data-driven mechanical fault diagnosis method for induction motors using stator current signals," *IEEE Trans. Transp. Electrif.,* vol. 9, no. 1, pp. 347-358, 2022.

[13] S. Nazari, S. Shokoohi, and J. Moshtagh, "A current noise cancellation method based on integration of stator synchronized currents for bearing fault diagnosis," *IEEE Trans. Instrum. Meas.,* vol. 73, pp. 1-8, 2023.

[14] M. R. Shahriar, P. Borghesani, and A. C. Tan, "Electrical signature analysis-based detection of external bearing faults in electromechanical drivetrains," *IEEE Transactions on Industrial Electronics,* vol. 65, no. 7, pp. 5941-5950, 2017.

[15] X. Chen, and Z. Feng, "New Schemes of Induction Motor Electric Signature Analysis for Gear Fault Diagnosis: A Comparative Study," *IEEE Transactions on Power Electronics*, vol. 39, no. 3, pp. 3590-3600, 2024.

[16] Z. Feng, X. Chen, and M. J. Zuo, "Induction motor stator current AM-FM model and demodulation analysis for planetary gearbox fault diagnosis," *IEEE Transactions on industrial informatics,* vol. 15, no. 4, pp. 2386-2394, 2018.

[17] Q. Han, T. Wang, Z. Ding, X. Xu, and F. Chu, "Magnetic equivalent modeling of stator currents for localized fault detection of planetary gearboxes coupled to electric motors," *IEEE Transactions on Industrial Electronics,* vol. 68, no. 3, pp. 2575-2586, 2020.

[18] S. Singh, and N. Kumar, "Detection of bearing faults in mechanical systems using stator current monitoring," *IEEE Transactions on Industrial Informatics,* vol. 13, no. 3, pp. 1341-1349, 2016.

[19] J. Lee, S. Park, S. Kim, O.-K. Choi, and C.-J. Chun, "LiteFDNet: A Lightweight Network for Current Sensor-based Bearing Fault Diagnosis," *IEEE Access*, vol. 12, pp. 100493-100505, 2024.

[20] J. Luo, Y. Chen, Q. Huang, S. Zhang, and X. Zhang, "Joint application of VMD and IWOA-PNN for Gearbox Fault Classification via Current Signal," *IEEE Sensors Journal*, vol. 23, no. 12, pp. 13155-13164, 15,2023.

[21] S. Tang, S. Yuan, and Y. Zhu, "Deep learning-based intelligent fault diagnosis methods toward rotating machinery," *Ieee Access,* vol. 8, pp. 9335-9346, 2019.

[22] D. Wang, Y. Li, L. Jia, Y. Song, and T. Wen, "Attention-Based Bilinear Feature Fusion Method for Bearing Fault Diagnosis," *IEEE/ASME Transactions on Mechatronics*, vol. 28, no. 3, pp. 1695-1705, 2023.

[23] X. Hou, F. Du, K. Huang, J. Qiu, and X. Zhong, "A current-based fault diagnosis method for rotating machinery with limited Training samples," *IEEE Transactions on Instrumentation and Measurement*, vol. 72, pp. 1-14, 2023.

[24] F. Cipollini, L. Oneto, A. Coraddu, S. Savio, and D. Anguita, "Unintrusive monitoring of induction motors bearings via deep learning on stator currents," *Procedia computer science,* vol. 144, pp. 42-51, 2018.

[25] B. Guan, X. Bao, H. Qiu, and D. Yang, "Enhancing bearing fault diagnosis using motor current signals: A novel approach combining time shifting and CausalConvNets," *Measurement,* vol. 226, pp. 114049, 2024.

[26] G. Cablea, P. Granjon, and C. Bérenguer, "Three-phase electrical signals analysis for mechanical faults monitoring in rotating machine systems," *Mechanical Systems and Signal Processing,* vol. 92, pp. 278-292, 2017.

[27] M. Blodt, M. Chabert, J. Regnier, and J. Faucher, "Mechanical load fault detection in induction motors by stator current time-frequency analysis," *IEEE Transactions on Industry Applications,* vol. 42, no. 6, pp. 1454-1463, 2006.

[28] R. R. Schoen, T. G. Habetler, F. Kamran, and R. Bartfield, "Motor bearing damage detection using stator current monitoring," *IEEE transactions on industry applications,* vol. 31, no. 6, pp. 1274-1279, 1995.
[29] M. Blodt, P. Granjon, B. Raison, and G. Rostaing, "Models for bearing damage detection in induction motors using stator current monitoring," *IEEE transactions on industrial electronics,* vol. 55, no. 4, pp. 1813-1822, 2008.
[30] B. Trajin, J. Regnier, and J. Faucher, "Comparison between vibration and stator current analysis for the detection of bearing faults in asynchronous drives," *IET electric power applications,* vol. 4, no. 2, pp. 90-100, 2010.
[31] F. Jia, Y. Lei, L. Guo, J. Lin, and S. Xing, "A neural network constructed by deep learning technique and its application to intelligent fault diagnosis of machines," *Neurocomputing,* vol. 272, pp. 619-628, 2018.
[32] H.-C. Li, W.-Y. Wang, L. Pan, W. Li, Q. Du, and R. Tao, "Robust capsule network based on maximum correntropy criterion for hyperspectral image classification," *Ieee Journal of Selected Topics in Applied Earth Observations and Remote Sensing,* vol. 13, pp. 738-751, 2020.
[33] Z. Zhang, W. Jiang, J. Geng, X. Deng, and X. Li, "Fault diagnosis based on non-negative sparse constrained deep neural networks and Dempster–Shafer theory," *IEEE Access,* vol. 8, pp. 18182-18195, 2020.
[34] L. Van Der Maaten, "Accelerating t-SNE using tree-based algorithms," *The journal of machine learning research,* vol. 15, no. 1, pp. 3221-3245, 2014.

Zhao-Hua Liu (M'16，SM'2022) He received M.Sc. degree in computer science and engineering, and the PhD. degree in automatic control and electrical engineering from the Hunan University, China, in 2010 and 2012, respectively. He worked as a visiting researcher in the Department of Automatic Control and Systems Engineering at the University of Sheffield, United Kingdom, from 2015 to 2016.

He is currently a Professor with the School of Information and Electrical Engineering, Hunan University of Science and Technology, Xiangtan, China. His current research interests include computational intelligence and learning algorithms design, parameter estimation and control of permanent-magnet synchronous machine drives, and condition monitoring and fault diagnosis for power system.

Dr. Liu has published a monograph in the field of Biological immune system inspired hybrid intelligent algorithm and its applications, and published more than 40 research papers in refereed journals and conferences, including IEEE TRANSACTIONS/JOURNAL/MAGAZINE. He is a regular reviewer for several international journals and conferences.

Jun-Jie Long received B. Eng. degree in Automation from the Hunan university of science and technology, Xiang tan, China, in 2021. He is currently pursuing the M.S. degree in Control Science and Engineering, at Hunan University of Science and Technology, Xiangtan, China.

His current research interests include deep learning algorithm design and fault diagnosis of rotating machinery.

Hua-Liang Wei received the Ph.D. degrees in automatic control from The University of Sheffield, Sheffield, U.K., in 2004.

He is currently a senior lecturer with the Department of Automatic Control and Systems Engineering, The University of Sheffield, Sheffield, UK. His research focuses on evolutionary algorithms, identification and modelling for complex nonlinear systems, applications and developments of signal processing, system identification and data modelling to control engineering.

Kan Liu (M'14–SM'17) received the B.Eng. and Ph.D. degrees in automation from Hunan University, Changsha, China, in 2005 and 2011, respectively, and the Ph.D. degree in electronic and electrical engineering from the University of Sheffield, Sheffield, U.K., in 2013. From 2013 to 2016, he was a Research Associate with the Department of Electronics and Electrical Engineering, University of Sheffield. From 2016 to 2017, he was a Lecturer with the Control Systems Group of the Loughborough University.

He is currently a Professor of electro-mechanical engineering with the Hunan University. His research interests include parameters estimation and sensorless control of permanent magnet synchronous machine drives and compensation of inverter nonlinearity, for applications ranging from automotive engineering to servo system.

Ying-Jie Zhang received the Ph.D. degree in control theory and control engineering from Hunan University (HNU), Changsha, China, in 2005. From 2010 to 2011, he was a Visiting Scholar with the University of Oslo, Oslo, Norway. In 2018, he was a Visiting Scholar with the Department of Electrical and Computer Engineering, Technische Universität Dresden, Dresden, Germany.

He is currently a Professor and the Yuelu Scholar with the College of Computer Science and Electronic Engineering, HNU, where he is also the Director of the Institute of Industry Energy-Saving Control and Evaluation. His research interests include parameter/state estimation, modeling, intelligent control, energy optimization, and intelligent control with applications to hybrid electric and autonomous vehicles, and fault detection and diagnosis for rotating machines.

Xiao-Hua Li received the B.Eng. degree in computer science and engineering from the Hunan University of Science and Engineering, Yongzhou, China, in 2007 and the M.Sc. degree in computer science from Hunan University, Changsha, China, in 2010.

She is currently a Lecturer of computer science with the School of Information and Electrical Engineering, Hunan University of Science and Technology, Xiangtan, China. Her research interest includes evolutionary computation and machine learning.